

Absence of low-temperature phase transitions in epitaxial BaTiO₃ thin filmsD. A. Tenne,^{1,*} X. X. Xi,^{1,2,3} Y. L. Li,² L. Q. Chen,^{2,3} A. Soukiassian,² M. H. Zhu,^{1,†} A. R. James,^{1,‡} J. Lettieri,²
D. G. Schlom,^{2,3} W. Tian,⁴ and X. Q. Pan⁴¹*Department of Physics, the Pennsylvania State University, University Park, Pennsylvania 16802, USA*²*Department of Materials Science and Engineering, the Pennsylvania State University, University Park, Pennsylvania 16802, USA*³*Materials Research Institute, the Pennsylvania State University, University Park, Pennsylvania 16802, USA*⁴*Department of Materials Science and Engineering, the University of Michigan, Ann Arbor, Michigan 48109, USA*

(Received 14 January 2004; published 3 May 2004)

We have studied phase transitions in epitaxial BaTiO₃ thin films by Raman spectroscopy. The films are found to remain in a single ferroelectric phase over the temperature range from 5 to 325 K. The low-temperature phase transitions characteristic of bulk BaTiO₃ (tetragonal-orthorhombic-rhombohedral) are absent in the films. X-ray diffraction shows that the BaTiO₃ films are under tensile strain due to the thermal expansion mismatch with the buffer layer. A phase-field calculation of the phase diagram and domain structures in BaTiO₃ thin films predicts, without any *priori* assumption, that an orthorhombic phase with in-plane polarization is the thermodynamically stable phase for such values of tensile strain and temperature, consistent with the experimental Raman results.

DOI: 10.1103/PhysRevB.69.174101

PACS number(s): 77.84.Dy, 77.55.+f, 78.30.Hv, 63.70.+h

I. INTRODUCTION

Phase transitions in thin film ferroelectrics, which differ substantially from those in corresponding bulk materials, are of significant scientific and technological interest.^{1,2} Much effort has been devoted in recent years to the thermodynamics of domain structures and phase diagrams in ferroelectric thin films.^{3–6} Different approaches have been employed by various groups. For example, Pertsev *et al.*⁵ predicted a number of domain stability maps for BaTiO₃ and PbTiO₃ using thermodynamic calculations whereas Li *et al.*⁶ proposed a phase-field model to predict the dependence of domain structures on temperature and strain. Experimentally, enhancement of the paraelectric-ferroelectric phase transition temperature, T_c , by strain has been reported in epitaxial ferroelectric films.^{7–10} Recently, Streiffer *et al.* observed nanoscale 180° stripe domains in ferroelectric PbTiO₃ thin films.¹¹ Strain-induced ferroelectricity in SrTiO₃ thin films has been reported by Fuchs *et al.*¹² and Tikhomirov *et al.*¹³ In this paper, we present a Raman scattering study of BaTiO₃ films in the temperature range 5–320 K, which shows that the tetragonal-orthorhombic and orthorhombic-rhombohedral phase transitions characteristic for the bulk BaTiO₃ disappear completely in the thin films. Detailed structural characterizations of the films suggest that a tensile strain locks the films in a single ferroelectric phase. A comparison with the phase-field model calculation confirms that the orthorhombic phase with in-plane polarization is the stable phase in this strain and temperature range.

In bulk BaTiO₃, the crystal structure changes from cubic to tetragonal at 403 K, then to orthorhombic at 278 K, and to rhombohedral at 183 K.¹⁴ The cubic phase is paraelectric and the other phases are ferroelectric. Raman spectroscopy is a powerful tool to study phase transitions as the structural changes alter the vibrational spectra. Lattice dynamics and Raman spectra of single crystal and polycrystalline BaTiO₃ have been studied in detail.^{15–22} Raman studies of thin BaTiO₃ films²³ have mostly focused on the ferroelectric

phase transition from cubic to tetragonal phase above room temperature. In the present paper we focus on the temperature range 5–325 K.

II. EXPERIMENTAL RESULTS

The BaTiO₃ films studied in this work were grown by pulsed laser deposition on (001)SrTiO₃ and (001)LaAlO₃ substrates. Between the substrate and BaTiO₃ film a 0.3 μm thick conducting layer of SrRuO₃ was deposited to screen Raman signal from the substrate.²⁴ The thickness of the BaTiO₃ films was 1 μm. The deposition conditions of the BaTiO₃ and SrRuO₃ layers were the same as those described previously.²⁵ Both layers were deposited at the substrate temperature of 750 °C. The structural properties of the BaTiO₃/SrRuO₃ samples were characterized by x-ray diffraction and transmission electron microscopy (TEM). BaTiO₃ single crystal was obtained from MTI Corp. (Richmond, CA). Raman spectra were recorded using a SPEX Triplemate spectrometer equipped with a liquid-nitrogen-cooled multichannel coupled-charge-device detector. The 514.5 nm line of an Ar⁺ laser was used for excitation, and the laser power density was kept at a low level (≤ 30 W/cm²) to avoid heating of the sample. Raman spectra from the films were measured in backscattering geometry both in parallel $z(x,x)\bar{z}$ and perpendicular $z(x,y)\bar{z}$ polarization configurations (z direction is normal to the film plane). The measurements in the crystal were in backscattering geometries both along the c axis of the initial tetragonal phase [$z(x,x)\bar{z}$ and $z(x,y)\bar{z}$ geometries] and perpendicular to it [$x(z,z)\bar{x}$ and $x(z,y)\bar{x}$ geometries].

Figure 1 shows Raman spectra of (a) a BaTiO₃ single crystal and (b) a BaTiO₃ film grown on a SrTiO₃ substrate, both measured in the parallel polarization configuration, as a function of temperature. The spectra of the single crystal show clear changes attributed to the phase transitions. At low temperatures, in the rhombohedral phase, the most intensive

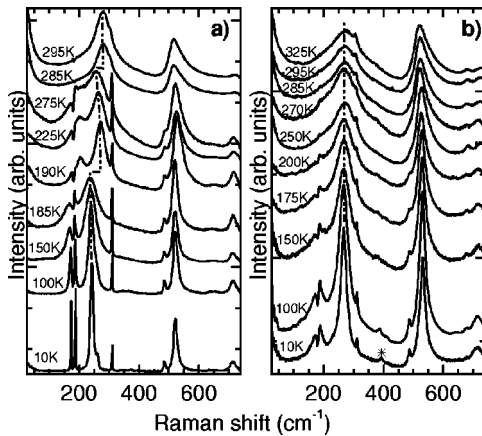


FIG. 1. Temperature evolution of Raman spectra of (a) a BaTiO₃ single crystal and (b) a BaTiO₃ film grown on SrTiO₃ substrate with a SrRuO₃ buffer layer, measured in parallel polarization geometry $z(x,x)\bar{z}$. Dashed-dotted lines are guides to eye. Star in the spectra of the film indicates features due to SrRuO₃ layer

lines observed in the polarized Raman spectrum are at 173, 187, 242, 485, 522, and 714 cm⁻¹, and are attributed to TO₁, LO₁, TO₂, LO₂, TO₃, LO₃ modes of A₁ symmetry, respectively.²⁰ The peak at 310 cm⁻¹ is due to mixed LO₂-TO₃ phonon of E symmetry.²⁰ The shoulder at 261 cm⁻¹ was shown by micro-Raman experiments to be due to the near-domain-wall regions of BaTiO₃ crystal.²² When the BaTiO₃ crystal was warmed to ~185 K, the Raman spectra went through large changes, most noticeable in the frequency range 150–300 cm⁻¹. Sudden jumps to a higher frequency, as large as 35 cm⁻¹ took place for the A₁ (TO₂) phonon line. A less dramatic, but still well pronounced jump (~10 cm⁻¹) occurred for the A₁ (TO₃) line. These changes are indicative of the rhombohedral-orthorhombic phase transition. When the crystal was heated further to ~280 K, another sudden jumps of the A₁ TO₂ and TO₃ phonon frequencies (25 and 4 cm⁻¹, respectively) and changes in the Raman spectra occurred, which indicates the orthorhombic-tetragonal phase transition. The observed frequency shifts are well detectable in Raman spectra despite large linewidths TO₂ and TO₃ phonons, and are in agreement with the reported results for BaTiO₃ crystals.^{15,21,22}

The temperature dependence of the Raman spectra of the BaTiO₃ film, shown in Fig. 1(b), is markedly different from that of the single crystal. It does not show sharp changes in the temperature range of 5–300 K. When temperature increases, the phonon lines broaden, but their frequencies are either almost constant (TO₂) or change only very slightly and gradually (TO₃). The two intensive sharp lines observed at 173 and 187 cm⁻¹ at low temperatures (rhombohedral phase) in the BaTiO₃ crystal are broader and their relative intensity is much smaller in the films at all temperatures measured. In fact, the positions, relative intensities and line shapes of phonon modes in the spectra of the films are similar to those of the orthorhombic phase of the single crystal.

The low-frequency range of Raman spectra (below 100 cm⁻¹) both in the crystals and thin films contains a feature of overdamped soft mode characteristic for

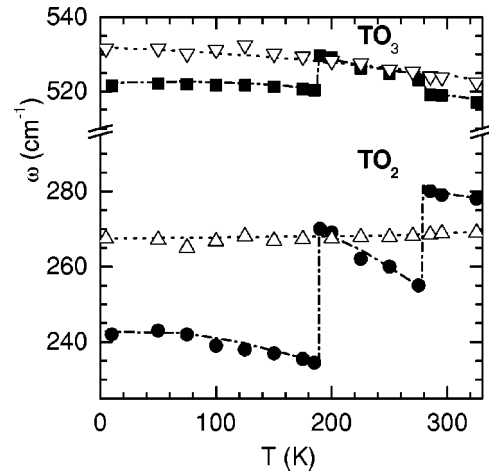


FIG. 2. Temperature dependence of the A₁ (TO₂) and A₁ (TO₃) phonon frequencies for BaTiO₃ single crystal (solid symbols) and film grown on SrTiO₃ substrate with SrRuO₃ buffer layer (open symbols).

BaTiO₃.^{16–18} The heavy overdamping of the soft mode in BaTiO₃ has been attributed to the order-disorder character of the phase transitions.²⁶ In the crystal overdamping is observed in the orthorhombic and tetragonal phases and increases with temperature, in agreement with earlier reported results.^{17,18} In thin films overdamping has also been observed to increase with temperature. However, no qualitative difference has been observed in the low-frequency Raman spectra of the films, as well as the crystals in the orthorhombic and tetragonal phases; there are no sharp changes in the overdamping behavior which would indicate the O-T phase transitions. Therefore, the behavior of the overdamped soft mode cannot be used to determine the phase transition temperature. So we focus on two hard phonon modes, TO₂ and TO₃, which exhibit most noticeable changes upon the rhombohedral-orthorhombic and orthorhombic-tetragonal phase transitions in BaTiO₃ crystals.

The temperature dependence of the frequencies of the A₁ (TO₂) and A₁ (TO₃) phonon modes for both the crystal and film shown in Fig. 2 clearly demonstrates the difference between the crystal and film behavior. Large jumps in the A₁ (TO₂) phonon frequency are clearly seen in the crystal, but it is constant in the film. The A₁ (TO₃) phonon frequency shows smaller jumps in the crystal, whereas no such jumps are visible in the film. This behavior indicates that the BaTiO₃ film does not undergo any phase transition in the temperature range 5–325 K. The same behavior was observed for films grown both on SrTiO₃ and LaAlO₃ substrates. The tetragonal-orthorhombic and orthorhombic-rhombohedral phase transitions of the bulk BaTiO₃ are completely absent in the thin films.

A quantitative determination of film strain is critical for the understanding of the complete disappearance of the low-temperature phase transitions. Figure 3 shows the x-ray diffraction results for a BaTiO₃/SrRuO₃ film on LaAlO₃ substrate. The θ -2 θ scan [Fig. 3(a)] shows that both the BaTiO₃ and SrRuO₃ layers grow with *c* axis normal to the substrate. The full width at half maximum (FWHM) values in 2 θ are

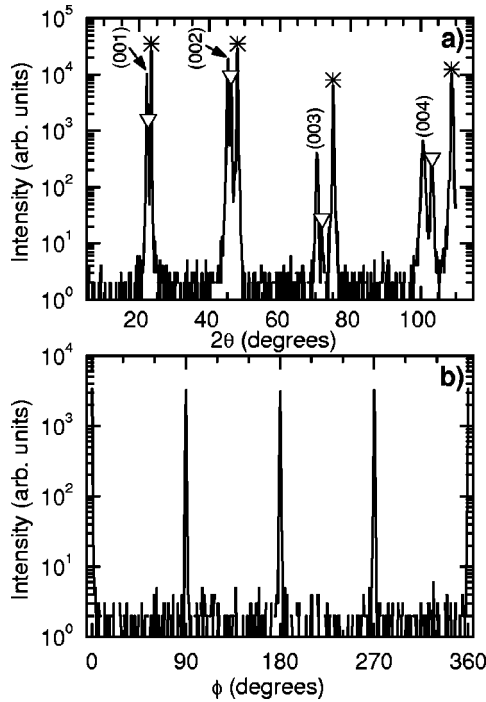


FIG. 3. X-ray diffraction patterns of BaTiO₃/SrRuO₃ film on LaAlO₃ substrate: (a) θ - 2θ scan; LaAlO₃ and SrRuO₃ peaks are marked by stars and down triangles, respectively. (b) ϕ scan of the BaTiO₃ 202 peak; $\phi=0^\circ$ is aligned to be parallel to the [100] in-plane direction of the LaAlO₃ substrate.

small (0.48° for the 003 peak). The ϕ scan of the BaTiO₃ 202 peak [Fig. 3(b)] shows that the layers are also in-plane aligned with the substrate lattice with $[100] \text{ BaTiO}_3 \parallel [100] \text{ SrRuO}_3 \parallel [100] \text{ LaAlO}_3$. The FWHM value for the 202 peak is 0.8° . From these scans, the lattice parameters of SrRuO₃ buffer layers are determined to be $a=3.93 \text{ \AA}$ for the pseudocubic lattice, equal to the bulk values. For BaTiO₃ films the measured lattice constants are $a=b=4.01 \pm 0.01 \text{ \AA}$ (in plane), and $c=4.004 \pm 0.001 \text{ \AA}$. Similar x-ray diffraction data were obtained for films grown on SrTiO₃ substrates, with the same epitaxial orientation, the same SrRuO₃ and BaTiO₃ lattice constants, and even smaller FWHM values (0.38° for 003 and 0.7° for 202 peaks).

TEM studies showed that the films consist of columnar grains with in-plane grain size of $\sim 100 \text{ nm}$. Electron diffraction results indicated the BaTiO₃ grains are oriented in same direction and confirmed the epitaxial relationship between the substrate, SrRuO₃ and BaTiO₃ layers described above. High crystalline quality of the films allows to presume the structural defects are unlikely to cause so drastic changes in the phase transition behavior. Although we cannot completely exclude other factors which can affect the film properties, such as composition fluctuations or grain size effect, we believe the strain in the thin films is the most probable cause of suppressing the low-temperature phase transitions characteristic for bulk BaTiO₃.

From the material parameters of BaTiO₃, the same as used by Koukhar *et al.* in Ref. 5, we calculated the lattice constants of the unstrained BaTiO₃ film to be $a_0=3.987 \text{ \AA}$

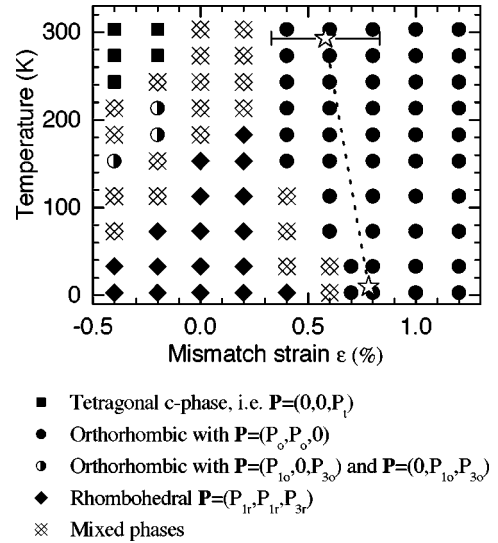


FIG. 4. Domain stability map for BaTiO₃ films under biaxial strain. The stars indicate the strain at room temperature, determined from x-ray data, and estimated strain at 5 K.

and $c_0=4.031 \text{ \AA}$, slightly different from those in the bulk BaTiO₃. Then from the measured lattice constants of our BaTiO₃ films the strain in the thin film $(a-a_0)/a_0$ is calculated to be a tensile strain of 0.58% . Although the lattice constants of both LaAlO₃ and SrTiO₃ substrates and of SrRuO₃ buffer layer are smaller than that of BaTiO₃, the misfit strain in our BaTiO₃ film is fully relaxed at the growth temperatures because the film thickness far exceeds the critical thickness for strain relaxation. The tensile strain arises from the mismatch between the thermal expansions of SrRuO₃ and BaTiO₃. The thermal expansion coefficient of SrRuO₃ (Ref. 27) is smaller than that of BaTiO₃.²⁸ Consequently, when a BaTiO₃ film is cooled to room temperature after the deposition, it contracts more than the SrRuO₃ buffer layer and a tensile stress is imposed on it. It is difficult to calculate the strain between 5–300 K because the thermal expansion coefficients of SrRuO₃ and BaTiO₃ are temperature dependent. It is, however, expected to increase when the temperature is lowered, which is schematically indicated by the dotted line in Fig. 4. The end point at 5 K (0.78%) was estimated by assuming the average thermal mismatch between SrRuO₃ and BaTiO₃ to be temperature independent.

III. PHASE-FIELD MODELING AND DOMAIN STABILITY MAP

We compare the film strain with the calculated phase diagram of BaTiO₃ films under biaxial substrate constraint and over the temperature range from room temperature to 0 K. The widely quoted phase diagram of Pertsev *et al.*⁵ assumes a simple domain structure with a particular domain wall orientation as *a priori* for the thermodynamic calculations. As a matter of fact, for BaTiO₃ films, three different domain stability maps have been presented, which depend on the assumptions of possible domain states and domain-wall orientations.⁵ In this work, we used a phase-field approach in which no *priori* assumption on the occurrence of certain

phases and domain structures is made.⁶ A brief description of the technique is as follows.

A ferroelectric domain structure is represented by the spatial distribution of the polarization field $\mathbf{P}=(P_1, P_2, P_3)$, and its temporal evolution is described by the time dependent Ginzburg-Landau (TDGL) equations,

$$\frac{\partial P_i(\mathbf{x}, t)}{\partial t} = -L \frac{\delta F}{\delta P_i(\mathbf{x}, t)} \quad (i=1,2,3), \quad (1)$$

where L is the kinetic coefficient related to the domain-wall mobility, and F is the total free energy of the system. $\mathbf{x}=(x_1, x_2, x_3)$ is a rectangular coordinate system and x_3 is normal to the film-substrate interface. The total free energy of the system includes the bulk free energy, the domain wall energy, and the elastic energy. The TDGL equation (1) was solved numerically using the semi-implicit Fourier-spectral method²⁹ for the time-stepping and spatial discretization. The macroscopic constraint of the substrate to the film is measured by the average strain $\bar{\epsilon}_{11}=\bar{\epsilon}_{22}=\epsilon$ and $\bar{\epsilon}_{12}=0$. The continuities of the deformation and stresses on film-substrate interface provide the local/microscopic constraint. By evolving Eq. (1) from an initial paraelectric state with small random perturbation, the thermodynamically stable domain structure and phase at given temperature and substrate constraint strain were obtained at the end of a simulation.

The results of the phase-field calculation for BaTiO₃ films are plotted in a phase diagram (domain stability map) shown in Fig. 4. The phases represented by various symbols are: solid squares—the tetragonal phases with polarization normal to the film/substrate interface, i.e., $\mathbf{P}=(0,0,\pm P_t)$; solid diamonds—the distorted rhombohedral phase with $\mathbf{P}=(\pm P_{1r}, \pm P_{1r}, \pm P_{3r})$; solid circles—the orthorhombic phase with polarization parallel to the film/substrate interface, i.e., $\mathbf{P}=(\pm P_o, \pm P_o, 0)$; and half-solid circles—the distorted orthorhombic phase with $\mathbf{P}=(\pm P_{1o}, 0, \pm P_{3o})$ or $\mathbf{P}=(0, \pm P_{1o}, \pm P_{3o})$. There are small regions, represented by crossed diamonds, within which more than one ferroelectric phases coexist. From this domain map, it is seen that a tensile strain of 0.58% places a BaTiO₃ film in the orthorhombic phase at room temperature. It should be noted that the uncertainty in the in-plane lattice parameter determined from x-ray data (0.01 Å) produces rather large uncertainty in the value of strain (shown by error bars on Fig. 4). Therefore, we

cannot absolutely rule out the possibility of existing mixed phases in the films at room temperature, if the lower uncertainty limit is taken into account. In the case of mixed orthorhombic-tetragonal phases there would be 90° domain walls at the boundaries between the orthorhombic phase with in-plane polarization and tetragonal phase polarized along c axis. However, the TEM images of our films showed the existence of many antiphase boundaries, but no 90° domains were found. Therefore, the films are most likely to be in the orthorhombic phase with in-plane polarization. This is confirmed by the Raman spectroscopy results (Figs. 1 and 2) as the form of the spectra, the phonon line positions and relative intensities in the BaTiO₃ film are close to those of the orthorhombic phase of BaTiO₃ single crystal. Because the tensile strain in the film increases when the temperature decreases from room temperature to 5 K, as schematically shown by the dotted line in Fig. 4, the film remains in the orthorhombic phase without undergoing any phase transitions.

IV. CONCLUSION

In summary, Raman spectroscopy in BaTiO₃ films grown by pulsed laser deposition on SrTiO₃ and LaAlO₃ substrates covered by SrRuO₃ buffer layers in the temperature range 5–325 K shows that the phase transitions between the different ferroelectric phases (tetragonal-orthorhombic-rhombohedral), characteristic of bulk BaTiO₃, are completely absent in the films. This behavior is explained by the presence of tensile strain in the BaTiO₃ film caused by thermal mismatch with the underlying SrRuO₃ layer. This is confirmed by a thin film phase diagram obtained from a phase-field calculation, which predicts, without any *priori* assumption, that the thermodynamically stable phase between 5–325 K for the experimentally determined value of tensile strain in the BaTiO₃ film is an orthorhombic phase with in-plane polarization.

ACKNOWLEDGMENTS

This work was partially supported by DOE under Grant Nos. DFFG02-84ER45095 (Xi) and DE-FG02-97ER45638 (Schlom), by DARPA under Grant No. MDA972-01-1-0023 (Xi) and by NSF under Grant Nos. DMR-01-22638 (Chen), DMR-9875405 and DMR-9871177 (Pan), and DMR-0103354 (Schlom, Chen, Xi).

*Electronic address: dat10@psu.edu; On leave from the Institute of Semiconductor Physics, Novosibirsk, Russia.

†Currently at Tsinghua University, Beijing, China.

‡Current address: Solid State Physics Laboratory, Lucknow Rd., Timarpur, Delhi-110 054, India.

¹S.K. Streiffer, C. Basceri, C.B. Parker, S.E. Lash, and A.I. Kingon, *J. Appl. Phys.* **86**, 4565 (1999).

²D. Damjanovic, *Rep. Prog. Phys.* **61**, 1267 (1998).

³J.S. Speck and W. Pompe, *J. Appl. Phys.* **76**, 466 (1994).

⁴A.L. Roytburd, *J. Appl. Phys.* **83**, 228 (1998); S.P. Alpay and A.L. Roytburd, *ibid.* **83**, 4714 (1998).

⁵N.A. Pertsev, A.G. Zembilgotov, and A.K. Tagantsev, *Phys. Rev. Lett.* **80**, 1988 (1998); N.A. Pertsev and V.G. Koukhar, *ibid.* **84**,

3722 (2000); V.G. Koukhar, N.A. Pertsev, and R. Waser, *Phys. Rev. B* **64**, 214103 (2001).

⁶Y.L. Li, S.Y. Hu, Z.K. Liu, and L.Q. Chen, *Appl. Phys. Lett.* **78**, 3878 (2001); Y.L. Li, S.Y. Hu, Z.K. Liu, and L.Q. Chen, *Acta Mater.* **50**, 395 (2002); L.Q. Chen, *Annu. Rev. Mater. Research* **32**, 113 (2002).

⁷Y. Yoneda, T. Okabe, K. Sakaue, H. Terauchi, H. Kasatani, and K. Deguchi, *J. Appl. Phys.* **83**, 2458 (1998).

⁸C.L. Li, Z.H. Chen, D.F. Cui, Y.L. Zhou, H.B. Lu, C. Dong, F. Wu, and H. Chen, *J. Appl. Phys.* **86**, 4555 (1999).

⁹K. Iijima, T. Terashima, K. Yamamoto, K. Hirata, and Y. Bando, *Appl. Phys. Lett.* **56**, 527 (1990).

¹⁰Yu. I. Yuzyuk, P. Simon, I.N. Zakharchenko, V.A. Alyoshin, and

- E.V. Sviridov, Phys. Rev. B **66**, 052103 (2002); Yu.I. Yuzyuk, J.L. Sauvajol, P. Simon, V.L. Lorman, V.A. Alyoshin, I.N. Zakharchenko, and E.V. Sviridov, J. Appl. Phys. **93**, 9930 (2003).
- ¹¹S.K. Streiffer, J.A. Eastman, D.D. Fong, C. Thompson, A. Munkholm, M.V. Ramana Murty, O. Auciello, G.R. Bai, and G.B. Stephenson, Phys. Rev. Lett. **89**, 067601 (2002).
- ¹²D. Fuchs, C.W. Schneider, R. Schneider, and H. Rietschel, J. Appl. Phys. **85**, 7362 (1999).
- ¹³O. Tikhomirov, H. Jiang, and J. Levy, Phys. Rev. Lett. **89**, 147601 (2002).
- ¹⁴*Landolt-Börnstein Numerical Data and Functional Relationships in Science and Technology, New Series, Group III* (Springer, Berlin, 1981), p. 67, Vol. 16.
- ¹⁵C.H. Perry and D.B. Hall, Phys. Rev. Lett. **15**, 700 (1965).
- ¹⁶M. DiDomenico, Jr., S.P.S. Porto, and S.H. Wemple, Phys. Rev. Lett. **19**, 855 (1967); M. DiDomenico, Jr., S.H. Wemple, S.P.S. Porto, and R.P. Bauman, Phys. Rev. **174**, 522 (1968).
- ¹⁷A. Scalabrin, A.S. Chaves, D.S. Shim, and S.P.S. Porto, Phys. Status Solidi B **79**, 731 (1977).
- ¹⁸G. Burns and F.H. Dacol, Phys. Rev. B **18**, 5750 (1978).
- ¹⁹H. Vogt, J.A. Sanjurjo, and G. Rossbroich, Phys. Rev. B **26**, 5904 (1982); H. Presting, J.A. Sanjurjo, and H. Vogt, *ibid.* **28**, 6097 (1983).
- ²⁰J.D. Freire and R.S. Katiyar, Phys. Rev. B **37**, 2074 (1988).
- ²¹U.D. Venkateswaran, V.M. Naik, and R. Naik, Phys. Rev. B **58**, 14 256 (1998).
- ²²M. Osada, M. Kakihana, S. Wada, T. Noma, and W.-S. Cho, Appl. Phys. Lett. **75**, 3393 (1999).
- ²³L.H. Robins, D.L. Kaiser, L.D. Rotter, P.K. Schenck, G.T. Stauf, and D. Rytz, J. Appl. Phys. **76**, 7487 (1994).
- ²⁴V.I. Merkulov, J.R. Fox, H.-C. Li, W. Si, A.A. Sirenko, and X.X. Xi, Appl. Phys. Lett. **72**, 3291 (1998).
- ²⁵D.A. Tenne, A.M. Clark, A.R. James, K. Chen, and X.X. Xi, Appl. Phys. Lett. **79**, 3836 (2001).
- ²⁶R.E. Cohen and H. Krakauer, Phys. Rev. B **42**, 6416 (1990).
- ²⁷J.J. Neumeier, A.L. Cornelius, and K. Andres, Phys. Rev. B **64**, 172406 (2001).
- ²⁸Y.S. Touloukian, R.K. Kirby, R.E. Taylor, and T.Y.R. Lee, *Thermal Expansion, Nonmetallic Solids, Thermophysical Properties of Matter* (Plenum, New York, 1977), Vol. 13.
- ²⁹L.Q. Chen and J. Shen, Comput. Phys. Commun. **108**, 147 (1998).